Microdrops on Atomic Force Microscope Cantilevers: Evaporation of Water and Spring Constant Calibration

Elmar Bonaccurso* and Hans-Jürgen Butt

Max-Planck-Institute for Polymer Research, Ackermannweg 10, 55128 Mainz, Germany

Received: June 30, 2004; In Final Form: October 20, 2004

The evaporation of water drops with radii $\sim$20 μm was investigated experimentally by depositing them onto atomic force microscope (AFM) cantilevers and measuring the deflection versus time. Because of the surface tension of the liquid, the Laplace pressure inside the drop, and the change of interfacial stress at the solid−liquid interface, the cantilever is deflected by typically a few hundred nanometers. The experimental results are in accordance with an analytic theory developed. The evaporation process could be monitored with high accuracy even at the last stage of evaporation because (1) cantilever deflections can be measured with nanometer resolution and (2) the time resolution, given by the inverse of the resonance frequency of the cantilever of $\sim$0.3 ms, is much faster than the typical evaporation time of 1 s. Experimental results indicate that evaporation of the last thin layer of water is significantly slower than the rest of the drop, which can be due to surface forces. This drop-on-cantilever system can also be used to analyze the drop impact dynamics on a surface and to determine the spring constant of cantilevers.

1. Introduction

Evaporation of drops from a solid surface is an everyday phenomenon. The rate of evaporation of a sessile drop on a solid surface gives hints on the interaction between a solid and a liquid, and it more generally consents to investigate surface and interface properties of solids, liquids, and gases. It is also relevant in technological processes, for example, heat transfer applications, the combustion of fuel, and prevention of degradation of coatings. For this reason, the dynamics of drop evaporation of pure liquids[1−8] or colloidal suspensions[9−13] on isothermal solid substrates is a vivid field of investigation.

Sessile drops on a solid surface can evaporate in three different modes:[5] (1) The contact area decreases while the contact angle remains constant, (2) the contact line is pinned so that the contact area remains constant while the contact angle decreases, or (3) both contact area and contact angle decrease at the same time. Also, mixed situations, with stick−slip motion of the receding contact line, were reported.[1,2,4]

Foremost, two methods have been applied to follow the evaporation process. First, the weight of the drop is continuously measured with an electronic microbalance[1,5] or with a quartz crystal microbalance (QCM),[12,14] and it is compared to the results of model calculations. The detection limit of a high-quality electronic microbalance (e.g., Sartorius CP2P) is around 10^{-6} g. That of a high-quality QCM is around 10^{-9} g, but QCM is sensitive to the precise drop position on the quartz crystal. Second, the dimensions of the drop are recorded with a video system of one or two cameras.[2,6,8,15] From the images, the contact radius, height, and contact angle are extracted and can be compared to theoretical predictions. The smallest drop sizes which have been analyzed are on the order of 10 μm.

An intriguing question is the dynamics of drop evaporation in its very last stages, when, for example, the Laplace pressure significantly increases, the vapor pressure according to the Kelvin equation increases, and surface effects play a predominant role. Neither the QCM nor video microscopy are suitable for tracking the evaporation to its very end, because the drops are too small.

In this manuscript, we present a technique which is particularly suitable to small drops. We placed liquid drops with a dispenser onto atomic force microscope cantilevers. The drop causes the cantilever to bend. This effect is also what causes an elastic solid surface to deform under a liquid drop.[16−18] We measured the deflection of the cantilever versus time. This deflection is sensitively related to the size of the drop, and so, the evaporation process can be traced. The aim of this study was to present the technique and a first analysis, to measure the evaporation rate of small water drops, and to characterize the micromechanical properties of cantilevers. Therefore, two kinds of experiments were performed (Figure 1):
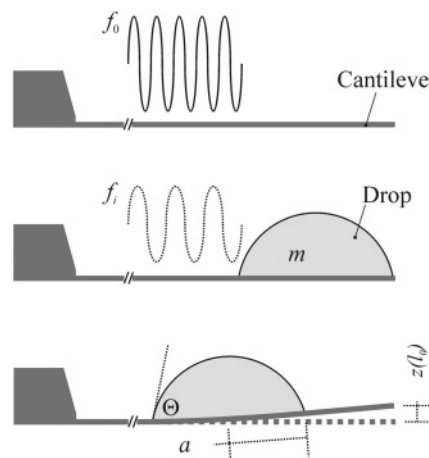

Figure 1. Schematic of the two kinds of measurements. The bare cantilever vibrates at its thermal resonance frequency f_0. When a drop of mass m is deposited close to its free end, the resonance frequency of the cantilever decreases to f_i. When a drop is deposited close to its fixed end, the main effect is that the cantilever deflects by a distance $z(l_0)$. Θ is the contact angle, and a the contact radius of the drop.

* Correspondence should be addressed to E.B. E-mail: bonaccur@mpip-mainz.mpg.de. Phone: 0049-6131-379 112. Fax: 0049-6131-379 310.

A drop of mass m is deposited close to the free end of a cantilever. As a consequence, the resonance frequency of the cantilever f decreased from f_0 to f_i. By monitoring the change of the resonance frequency during the evaporation, $m(t)$ can be obtained, assuming that the spring constant of the cantilever is known. On the other hand, knowledge of the mass of the deposited drop by imaging it with a video microscope allows us to calculate the spring constant.

A drop is deposited at a certain distance from the free end of a cantilever. In this case, we focused on the resulting deflection of the cantilever, which is directly related to the contact radius a and the contact angle Θ of the drop.

In this paper, we describe the experimental setup, we develop an analytic theory for describing the shape of the AFM cantilever in the presence of a drop, and we present and discuss the results.

2. Theory

To describe the process of deposition and evaporation of a microdrop from a cantilever, it is instructive to distinguish three time domains:

The drop hits the solid surface and spreads until it has reached its maximal contact radius and takes the shape of a spherical cap. This spreading process is characterized by a time constant τ_s. On the basis of results of von Bahr et al.[19] and Rioboo et al.,[20] we estimate that this process is finished after typically 1 ms. This process is the most complex of the three. When a drop of a liquid hits a surface, it is deformed and, depending also on the liquid−solid interaction, the drop might splash and lose part of its mass.[21] The kinetic energy of the drop is partly transformed into the surface energy of the expanding liquid−vapor interface, partly dissipated due to viscous forces inside the drop and partly transferred to the cantilever as elastic energy. After impact, the drop oscillates with a characteristic frequency $f_s = \sqrt{\gamma/\rho V}$, where γ is the surface tension of the liquid, ρ is the density, and V is the volume of the drop.[19] This oscillation is damped with a time constant $\tau_s = \rho V^{2/3}/\eta$ due to viscous dissipation, where η is the viscosity of the drop. For a typical water drop with a diameter of 40 μm, $\gamma = 0.072$ N/m, $\rho = 1000$ kg/m³, $\eta = 0.95$ mPa s, we find that $f_s \approx 49$ kHz and $\tau_s \approx 1$ ms. Because the cantilevers we used have resonance frequencies lower than f_s, it is not possible for us to record the drop oscillation, but we are able to record the damping time. Nevertheless, the oscillating drop might excite the cantilever to other vibration modes.

The impact of the drop causes the cantilever to vibrate. The initial vibration is damped, and the amplitude decays exponentially with a time constant τ_d, which is between 2 and 10 ms in air.

Finally, the drop evaporates from the cantilever. The evaporation of the drop, characterized by τ_e, takes on the order of 1 s.

The three time domains are different, which allows us to treat them separately. Here, we describe the bending of the cantilever during the second and third processes. In all cases, a rectangular cantilever of total length l_0, width w, and thickness d is considered. The drop is assumed to be much smaller than its capillary length, so that its shape is that of a spherical cap with a radius R.

2.1. Initial Vibration of the Cantilever. When the drop hits the surface, momentum is transferred to the cantilever. In the following description, we assume that $\tau_s \ll \tau_d$ and that momentum is effectively transferred at $t = 0$. The cantilever starts to vibrate until damping brings it to rest. This process

can be described by the equation of motion

$$m*\frac{d^2z}{dt^2} + D\frac{dz}{dt} + Kz = 0 \tag{1}$$

assuming that no external forces are acting and neglecting gravitation. Here, D is a damping coefficient, and $m*$ is the effective mass of the cantilever. Equation 1 is valid for the deflection of the cantilever at its end, $z(x = l_0)$, and is independent of its form. For a rectangular cantilever, the spring constant is

$$K = \frac{Ewd^3}{4l_0^3} \tag{2}$$

where E is Young's modulus, and the effective mass is

$$m* = m + 0.243M \tag{3}$$

Here, m is the mass of the drop, and M is the mass of the cantilever.[22] We assume that the drop is positioned at the free end of the cantilever and that the cantilever vibrates in its first vibration mode (for details, see refs 23 and 24). One of the cantilevers had, for example, a length of 470 μm, a width of 50 μm, and a thickness of 2 μm. With a density of 2330 kg/m³ (silicon), we get $M = 1.1 \times 10^{-10}$ kg. This is equal to the mass of a water drop with a 30-μm radius.

The general solution of eq 1 is

$$z(t) = -A_0 \cdot \sin(\omega t + \varphi) \cdot e^{-t/\tau_d} \tag{4}$$

with

$$\omega = 2\pi f = \sqrt{\frac{K}{m*}} \tag{5}$$

and $\tau_d = 2m*/D$. Initially, the deflection of the cantilever is zero, $z(t = 0) = 0$, which leads to $\varphi = 0$. The negative sign in eq 4 takes into account that the falling drop causes the cantilever first to bend downward.

To estimate the amplitude A_0, we use the conservation of momentum and assume that the momentum of the cantilever plus drop after impact is equal to the momentum of the falling drop before it hits the cantilever. This leads to

$$m*\frac{dz}{dt}(t = 0) \approx m_i v_0 \tag{6}$$

where v_0 and m_i are the velocity and mass of the drop before impact. Equation 6 is only an approximation, because due to the impact, not only first, but also higher, vibration modes might be excited. With this condition, the amplitude of the vibration is proportional to the momentum of the falling drop

$$A_0 \approx \frac{m_i v_0}{m* 2\pi f_i} \tag{7}$$

The mass of the drop was measured by optical methods. For a rectangular cantilever, using eqs 3 and 5, we can calculate the spring constant from the initial resonance frequency of the cantilever with the drop

$$f_i = \frac{1}{2\pi}\sqrt{K/(m_i + 0.243M)} \tag{8}$$

and the resonance frequency without the drop

$$f_0 = \frac{1}{2\pi} \sqrt{\frac{K}{0.243M}} = 0.323 \frac{d}{l_0^2} \sqrt{\frac{E}{\rho}} \tag{9}$$

This is analogous to the method proposed by Cleveland et al.,[25] who attached defined masses to the ends of cantilevers to measure K.

We assumed that liquid evaporation is negligible at time scales on the order of τ_d. This is not precisely true: In reality, a small but detectable amount of liquid evaporates in this time span. For this reason, the mass of the drop and, thus, m^* decreases while f increases. This is noticeable in a frequency shift during the initial vibration. To take this reduction of the mass into account, a linear term was subtracted from the mass:

$$f(t) = \frac{1}{2\pi} \sqrt{\frac{K}{m_i + 0.243M - \alpha t}} \tag{10}$$

Here, α is the initial evaporation rate in kg/s. By writing this in a series and taking only the linear term into account, the increase in frequency for $t \ll \tau_e$ is

$$f = f_i + \frac{\alpha f_i^3}{2K} t \tag{11}$$

Practically, one can plot the inverse of the period for one vibration versus time. From the slope of the linear increase, we get $\alpha f_i^3/(2K)$. By knowing f_i and K, the initial rate of evaporation can be determined.

2.2. Evaporation of the Drop. Here, we calculate the shape of a cantilever induced by a drop sitting on the top side for $t \gg \tau_d$. We assume that the bending of the cantilever takes place at a slower time scale than the inverse resonance frequency, so that the cantilever is always in equilibrium with respect to a given drop shape.

Several effects can cause a deflection of the cantilever: (1) The normal component of the surface tension of the liquid and the Laplace pressure in the drop, (2) the change in interfacial stress when the solid−vapor surface is replaced by a solid− liquid interface, (3) the lateral component of the surface tension of the liquid, (4) the line tension at the periphery of the drop, and (5) the gravitational force due to the weight of the drop.

In the following, we discuss the effect of all contributions on the cantilever shape. First, the shape of the cantilever in a Cartesian coordinate system XYZ is calculated. This coordinate system originates in the center of the contact area of the drop (Figure 2). The X axis is oriented along the cantilever parallel to the cantilever surfaces in the center of the drop. As the most relevant property, the inclination at the rim of the drop is derived. The resulting change in cantilever shape is supposed to be very small compared to the size of the drop. In a second step, we consider the shape of the whole cantilever, transforming the results to the coordinate system xyz, which originates at the base of the cantilever with a horizontal x axis.

2.2.1. Normal Component of Liquid Surface Tension and Laplace Pressure. A sitting liquid drop exerts a pressure, the Laplace pressure, to the surface of the solid plate. This pressure is

$$P = \frac{2\gamma}{R} = \frac{2\gamma \sin \Theta}{a} \tag{12}$$

Here, R is the radius of curvature of the drop, a is the radius of the contact area, and Θ is the contact angle. At the rim of the drop, we have an additional force per unit length due to the surface tension of the liquid. The normal component of this
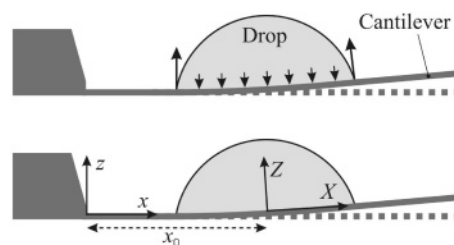

Figure 2. Side view of a drop placed on a cantilever which is fixed on the left side. It exerts a Laplace pressure over the whole contact area and a force due to the surface tension of the liquid at the three-phase contact line. Bottom: Coordinate systems used. Dimensions are not to scale.
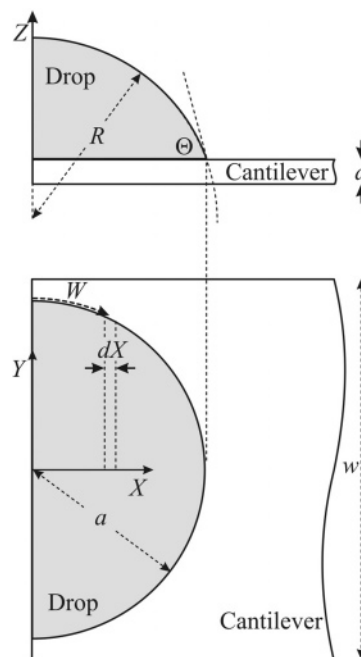

Figure 3. Side and top view schematics of a plate with a drop in its center. Only one-half of the drop is shown.

force (per unit length) is directed upward and given by $\gamma' = \gamma \sin \Theta$. These forces cause a torque which is opposed by the elastic response of the cantilever.

We divide the cantilever in infinitesimal thin stripes parallel to the Y axis (Figure 3). At a given X position on the cantilever, the torque is given by

$$M(X) = 2 \cdot \int_X^a (X' - X)\left[\gamma' \frac{dW}{dX'} - PY\right] dX' \tag{13}$$

The factor $(X' - X)$ is the lever of the force acting at X'. Here, W is the length of the three-phase contact line corresponding to a given value of X. The force due to the surface tension of the liquid acting on a stripe of width dX' is $2\gamma' \cdot dW/dX' \cdot dX'$. The factor two is caused by the fact that the surface tension is acting at Y and $-Y$. The Laplace pressure causes a force $2PY \cdot dX'$. With

$$W = a \cdot \arctan\left(\frac{X}{\sqrt{a^2 - X^2}}\right) \tag{14}$$

the torque is

$$M(X) = 2 \int_X^a (X' - X) \left[\frac{a\gamma'}{\sqrt{a^2 - X'^2}} - \frac{2\gamma'}{a} \sqrt{a^2 - X'^2} \right] dX' =$$
$$\frac{2\gamma'}{3a} (a^2 - X^2)^{3/2} \quad (15)$$

This torque is compensated by the restoring elastic response of the cantilever, which is described by $EI \cdot d^2Z/dX^2$, where

$$I = wd^3/12 \quad (16)$$

Considering both contributions, we get the differential equation

$$\frac{d^2Z}{dX^2} = \frac{2\gamma'}{3EIa} (a^2 - X^2)^{3/2} \quad (17)$$

$Z(X)$ describes the shape of the cantilever in the XYZ coordinate system. Integration with the boundary condition $dZ/dX = 0$ at $X = 0$ leads to the inclination

$$\frac{dZ}{dX} = \frac{2\gamma'}{3EIa} \left[\frac{X}{4} (a^2 - X^2)^{3/2} + \frac{3}{8} a^2 X \sqrt{a^2 - X^2} + \frac{3a^4}{8} \arctan\left(\frac{X}{\sqrt{a^2 - X^2}}\right) \right] \quad (18)$$

The inclination at the end of the drop ($X = a$) is

$$\frac{dZ}{dX} = \frac{\pi a^3 \gamma \sin \Theta}{8EI} \quad (19)$$

For completeness, we integrate eq 17 a second time with $Z = 0$ at $X = 0$ to get the deflection

$$Z = \frac{2\gamma'}{3EIa} \left[-\frac{1}{20} (a^2 - X^2)^{5/2} + \frac{1}{8} a^2 X^2 \sqrt{a^2 - X^2} + \frac{3a^4 X}{8} \arctan\left(\frac{X}{\sqrt{a^2 - X^2}}\right) + \frac{a^4}{4} \sqrt{a^2 - X^2} - \frac{a^5}{5} \right] \quad (20)$$

At $X = a$, this reduces to

$$Z = \frac{2\gamma' a^4}{3EI} \cdot \left(\frac{3\pi}{16} - \frac{1}{5} \right) = 0.2594 \cdot \frac{a^4 \gamma \sin \Theta}{EI} \quad (21)$$

The Laplace pressure and the normal component of the surface tension of the liquid are the dominant factors for cantilever bending.

2.2.2. Change in Surface Stress. Another contribution to the bending of the cantilever is the change in surface stress $\Delta\sigma$. In the contact area, solid−vapor surface is replaced by solid−liquid interface. This results in a change in surface stress and generates a constant torque over the whole contact area. Usually, the surface stress is reduced by a liquid, which leads to a bending away from the drop. If the whole surface of the cantilever would be covered, the bending would be described by Stoneys formula.[26] In our case, only the contact area contributes.

The torque at a given position X is

$$M = -\Delta\sigma Y(X)d = -\Delta\sigma d \sqrt{a^2 - X^2} \quad (22)$$

In this case, the factor of two, which takes into account the contribution from $-Y$ to Y, is compensated by the fact that the lever of the torque is only $d/2$. The minus sign indicates that the cantilever bends away from the drop. This leads to

$$\frac{d^2Z}{dX^2} = -\frac{\Delta\sigma \cdot d}{EI} \sqrt{a^2 - X^2} \quad \text{for } X \le a \quad (23)$$

First integration leads to the inclination

$$\frac{dZ}{dX} = -\frac{\Delta\sigma \cdot d}{2EI} \left[X\sqrt{a^2 - X^2} + a^2 \arctan\left(\frac{X}{\sqrt{a^2 - X^2}}\right) \right] \quad (24)$$

A second integration gives the deflection

$$Z(X) = -\frac{\Delta\sigma \cdot d}{2EI} \left[\frac{2a^2 + X^2}{3} \sqrt{a^2 - X^2} + a^2 X \arctan\left(\frac{X}{\sqrt{a^2 - X^2}}\right) - \frac{2a^3}{3} \right] \quad (25)$$

At $X = a$, we have

$$\frac{dZ}{dX} = -\frac{\pi \Delta\sigma a^2 d}{4EI} \quad (26)$$

and

$$Z = -\frac{\Delta\sigma a^3 d}{4EI} \left(\pi - \frac{4}{3} \right) \quad (27)$$

2.2.3. Lateral Component of Liquid Surface Tension. The surface tension of the liquid also has a component parallel to the cantilever surface, which is $\gamma \cos \Theta$. This causes a contraction (for $\Theta < 90°$) or expansion (for $\Theta > 90°$) of the top surface and, thus, a bending of the cantilever.

The torque due to the lateral component of the liquid surface tension is given by

$$M(X) = \gamma d \sqrt{a^2 - X^2} \cdot \cos \Theta \quad (28)$$

This is similar to eq 22 if we replace $-\Delta\sigma$ by $\gamma \cos \Theta$, and we can directly write the result:

$$\frac{dZ}{dX} = \frac{d\gamma \cos \Theta}{2EI} \left[X\sqrt{a^2 - X^2} + a^2 \arctan\left(\frac{X}{\sqrt{a^2 - X^2}}\right) \right] \quad (29)$$

$$Z(X) = \frac{d\gamma \cos \Theta}{2EI} \left[\frac{2a^2 + X^2}{3} \sqrt{a^2 - X^2} + a^2 X \arctan\left(\frac{X}{\sqrt{a^2 - X^2}}\right) - \frac{2a^3}{3} \right] \quad (30)$$

At the end ($X = a$), we obtain an inclination of

$$\frac{dZ}{dX} = \frac{\pi a^2 d\gamma \cos \Theta}{4EI} \quad (31)$$

and a deflection

$$Z = \frac{a^3 d\gamma \cos \Theta}{4EI} \left(\pi - \frac{4}{3} \right) \quad (32)$$

In equilibrium, that is, if the three-phase contact line is not moving and line pinning is negligible, we can apply Young's equation, $\gamma \cos \Theta = \gamma_S - \gamma_{SL}$. Here, γ_S and γ_{SL} are the surface tensions of the solid−vapor and solid−liquid interfaces, respectively. This leads to the conclusion that this component should exactly compensate the effect of surface stress if $\Delta\sigma = \gamma_S - \gamma_{SL}$. The net effect of surface stress and the lateral

Microdrops on AFM Cantilevers

J. Phys. Chem. B, Vol. 109, No. 1, 2005 **257**

component of the surface tension is thus

$$\frac{dZ}{dX} = \frac{\pi a^2 d}{4EI} (\gamma \cos \Theta - \Delta\sigma) \quad \text{for } X \geq a \qquad (33)$$

Usually, the bending due to the Laplace pressure and the normal component of the surface tension dominate. Only for small contact angles can the combined effect of the lateral component of the liquid surface tension and the surface stress possibly lead to a significant effect. This can easily be seen after dividing eq 33 by eq 19. The result

$$\frac{d}{a} \cdot \frac{\cos \Theta - \Delta\sigma/\gamma}{\sin \Theta}$$

is usually much smaller than unity, because $d/a \ll 1$, unless the contact angle is small.

2.2.4. Line Tension. If energy is required (released) to form the three-phase contact line, that effect tends to contract (expand) the periphery of the drop. At a given position X, the line tension κ contracts the top side of the cantilever with a force $2\kappa \sqrt{a^2 - x^2}/a$. The lever is $d/2$. The torque due to the line tension of a circular ring on a cantilever is therefore

$$M = \frac{\kappa d}{a} \sqrt{a^2 - X^2} \quad \text{for } X \leq a \qquad (34)$$

Again, this is similar to eq 22 if we replace $-\Delta\sigma$ by κ/a. The resulting inclination at the end is

$$\frac{dZ}{dX} = \frac{\pi a \kappa d}{4EI} \quad \text{for } X \geq a \qquad (35)$$

To estimate the effect of line tension, we divide eq 35 by eq 19 and obtain

$$\frac{d}{a} \cdot \frac{2\kappa}{a\gamma \sin \Theta}$$

Unless the contact angle is small, this is usually much smaller than unity, because $d/a \ll 1$ and typically $a\gamma$ is on the order of 10^{-7} N, which is much larger than normal line tensions, which are below 10^{-8} N.

2.2.5. Effect of Gravitation. The gravitational force due to the weight of the drop is small and has been described before (e.g., ref 27). Even the largest drops ($R = 30$ μm) lead to a gravitational force of only 1.1 nN, which for a cantilever with $K = 0.2$ N/m leads to a downward (negative) deflection at the end of 5.5 nm. The effects discussed here are much larger, and we neglected gravitation.

2.2.6. Considering the Whole Cantilever. Until now, all results were given in the coordinate system XYZ which originates in the center of the contact area of the drop. In the coordinate system xyz, x is parallel to the cantilever at its base and oriented horizontally. The drop is centered at x_0. For $x \leq x_0 - a$, deflection and inclination are zero ($dz/dx = 0$, $z = 0$). For $x \geq x_0 + a$, the inclination is given by twice dZ/dX, leading to

$$\frac{dz}{dx} = \frac{\pi a^3}{4EI}\left[\gamma \sin \Theta + \frac{2d}{a}\left(\gamma \cos \Theta - \Delta\sigma + \frac{\kappa}{a}\right)\right] \qquad (36)$$

Here, $z(x)$ describes the shape of the cantilever. The first term is caused by the Laplace pressure and the normal component of the liquid surface tension. It leads to an upward bending of the cantilever toward the drop. The second term disappears for $\Delta\sigma = \gamma_S - \gamma_{SL}$, that is, when Young's equation is valid and
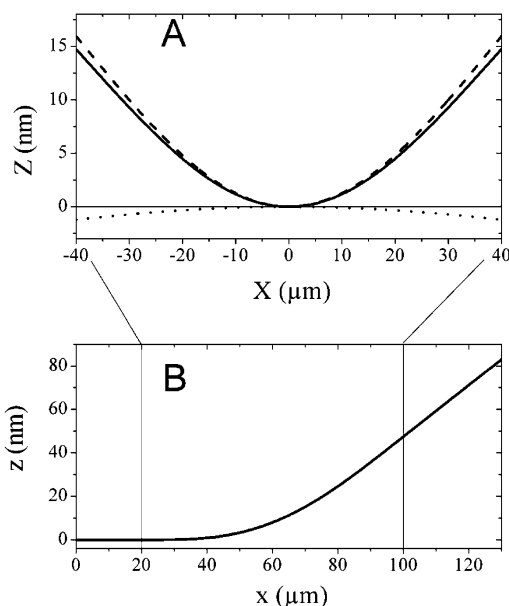

Figure 4. Shape of a cantilever with a drop on top calculated for a rectangular cantilever with typical dimensions (width $w = 100$ μm, thickness $d = 1$ μm) with a typical water drop (contact angle $\Theta = 30°$, contact radius $a = 40$ μm) on top using eqs 20, 25, and 30. Side views of the cantilever are shown in the coordinates XYZ (A) and in laboratory coordinates xyz (B). Continuous lines show the total shape. The dashed line shows the effect of the Laplace pressure and surface tension (eq 20). The dotted line shows the effect of the surface stress plus lateral component of the liquid surface tension with $\Delta\sigma - \gamma \cos \Theta = 0.06$ N/m (eqs 25 and 30). Please note the different scales used for the horizontal and vertical axes.

the difference in the solid surface tensions is equal to the change in surface stress. The last term is expected to be small, so that we can approximately write

$$\frac{dz}{dx} \approx \frac{\pi a^3}{4EI} \gamma \sin \Theta \quad \text{for } x \geq x_0 + a \qquad (37)$$

The deflection is approximately (that is, if x is much larger than $x_0 + a$) given by

$$z(x) \approx \frac{dz}{dx}(x - x_0) \qquad (38)$$

In Figure 4, the shape of a cantilever in both coordinate systems is shown. Typical parameters for the drop ($a = 40$ μm, $\Theta = 30°$) and cantilever were assumed. The strongest bending is below the center of the drop. It is also obvious that the contribution of surface stress is small even though we assumed a relatively high value of $\Delta\sigma - \gamma \cos \Theta = 0.06$ N/m.

2.2.7. Taking the Calibration of Cantilever Deflection into Account. In commercial AFMs, the inclination at the end of the cantilever is measured by the optical lever technique. Inclination is usually converted to deflection by pushing the end of the cantilever upward by a defined distance. If we apply a force at its end, the shape of the cantilever is described by a third-order polynomial. Deflection $z(l_0)$ and inclination dz/dx ($x = l_0$) are related by[28]

$$\frac{dz}{dx}(l_0) = \frac{3}{2l_0} z(l_0) \qquad (39)$$

An example is shown to demonstrate that at the same deflection $z(l_0)$ the inclination dz/dx ($x = l_0$) is different (Figure 5).
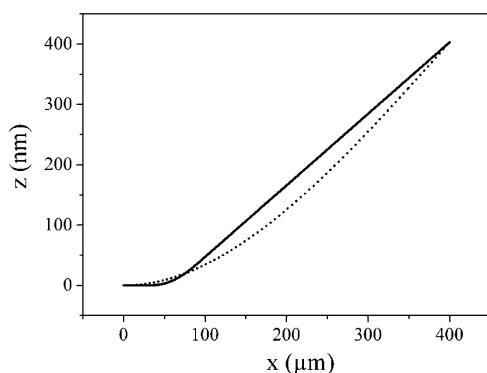
Figure 5. Comparison of a cantilever deflected by a drop on top (continuous line) and a cantilever deflected by a force of $F = 28$ nN at its end (dashed line) calculated with $z = F/(2EI) \cdot (l_0 x^2 - x^3/3)$.[22] The force was chosen so that the resulting deflection is similar to the one caused by the drop. The parameters to calculate the effect of the drop were $d = 1$ μm, $w = 100$ μm, $a = 40$ μm, and $\Theta = 30°$. The length of the cantilever was assumed to be $l_0 = 400$ μm. The center of the drop is placed $x_0 = 60$ μm away from the base.
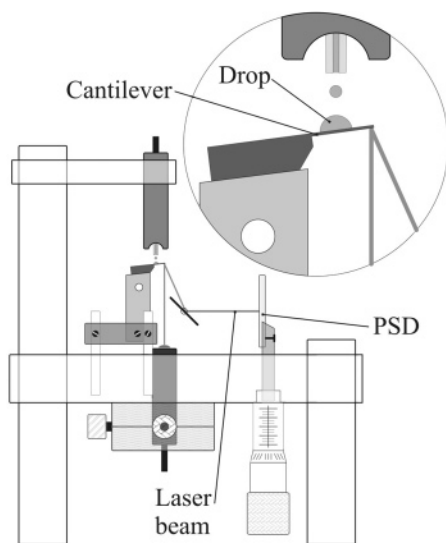

Figure 6. Experimental setup for monitoring the drop evaporation, with a blowup showing the drop−cantilever system in detail. The drop is generated by a nozzle and impacts on the cantilever from above. The deflection of the cantilever is measured with a laser from below with the light lever technique, a position-sensitive device (PSD) tracking the movement of the laser. The video microscope is directed perpendicularly to the plane of the figure.

3. Experimental Methods

We used an inverted and modified particle interaction apparatus[29] to measure the evaporation rate of a water drop (Figure 6). Water drops of diameters between 40 and 60 μm (milliQ, Millipore Corp., U.S.A.) were generated by a microdrop system (Microdrop GmbH, Norderstedt, Germany). A three-axes hydraulic micromanipulator (MMO-203, Narishige Co. Ltd., Japan) was used for depositing the drops on the desired place on a horizontally mounted micromachined cantilever (soft "octosensis" cantilevers from Micromotive GmbH, Mainz, Germany; stiff "pointprobe" cantilevers from NanoWorld GmbH, Erlangen, Germany). Typical dimensions of the soft rectangular silicon cantilevers were $l_0 = 750$ μm, $w = 100$ μm, $d = 0.89$ μm, $K = 0.007$ N/m (±0.002 N/m), and $f_0 = 2.12$ kHz, and of the stiff rectangular silicon cantilevers were $l_0 = 470$ μm, $w = 50$ μm, $d = 2$ μm, $K = 0.20$ N/m (±0.03 N/m), and $f_0 = 11.86$ kHz. Cantilever spring constants were measured

with the MFP-1D (Asylum Research, Santa Barbara, CA) applying the thermal noise method.[23,30]

The deposition of a drop causes the cantilever to bend. This bending is measured by the light lever technique commonly used in AFM, pointing a laser beam at the free end of the cantilever and detecting the position of the reflected beam. Cantilever deflections could be measured with nanometer accuracy.

We modified one or both faces of the cantilevers in order to obtain different surface energies. The first batch of cantilevers was used as received. The second batch was gold-coated on the top side (the side in contact with the drop, layer thickness of 22 nm). The third batch was silanized on both sides with OTS (octadecyltrichlorosilane). Therefore, cantilevers were first cleaned in a solution of water/ammonium hydroxide/hydrogen peroxide (5/1/1 vol %). Then, they were immersed overnight in a solution of decalin/tetrachlorocarbon/chloroform (7/2/1 vol %) added with 1 vol % OTS.

The contours of the drops on cantilevers were monitored with a video microscope (Precise Eye, Navitar, NY, U.S.A.) from the side in combination with a frame grabber and a CCD camera (WAT-202D, Watec Co. Ltd., Japan). We used a 34-mm working distance, 5× objective (Mitutoyo Corp, Kawasaki, Japan), which, in combination with the Navitar microscope, was capable of a magnification up to 450×. The resolution of a single frame was 640 × 480 pixels;[2] the frame rate was 25 frames per second (fps). From video images, the contact radius and contact angle of the drops were obtained. We further used a stereo microscope from the front as a help for centering the drop on the longitudinal axis of the cantilever. An average drop takes around one second to evaporate, so that typically 25 frames were analyzed for each experiment. We fitted a circle to each drop of each frame for controlling the profile of the drop cap so that it was indeed circular. From the fit, we obtained the radius of curvature R, the contact radius a, and the height h of the drop cap. From a and h, the contact angle and drop volume were calculated by $\Theta = 2 \arctan(h/a)$ and $V = \pi h(3a^2 + h^2)/6$. The drop evaporation took place at a temperature of 22 (±1) °C and a relative humidity of 40 (±5)%.

4. Results and Discussion

4.1. Drop at the End of the Cantilever. *4.1.1. Spring Constant of Cantilevers.* Figure 7 shows a typical sequence of five successive microscope pictures taken from the side. After the drop leaves the dispenser, it takes a spherical shape as it is falling toward the cantilever (Figure 7 top). The second picture from the top ($t \approx 0$) shows the drop after impact. The initial vibration of the cantilever causes the image to be slightly blurry. As the sequence was taken at 25 fps, the interval between two consecutive pictures is 40 ms, and the initial vibration only takes ~10 ms. After 40 ms, the drop has equilibrated and is evaporating: The rim of the drop is pinned (the contact radius remains constant), but the drop height decreases slightly from 20 to 19.5 μm. In this particular case, the drop remained pinned for almost the whole evaporation process, as is shown in the fourth picture taken after 600 ms: The contact radius decreases only slightly, while the drop height decreases significantly. The last picture is taken just before the drop has completely evaporated.

Different types of cantilevers respond differently to impacting drops (Figure 8). The graph at the top (Figure 8A) is for a stiff silicon cantilever like that shown in Figure 7, having a tip protruding about 15 μm off the surface. The drop contact angle with the cantilever is about 62° after equilibration. The graph

Microdrops on AFM Cantilevers

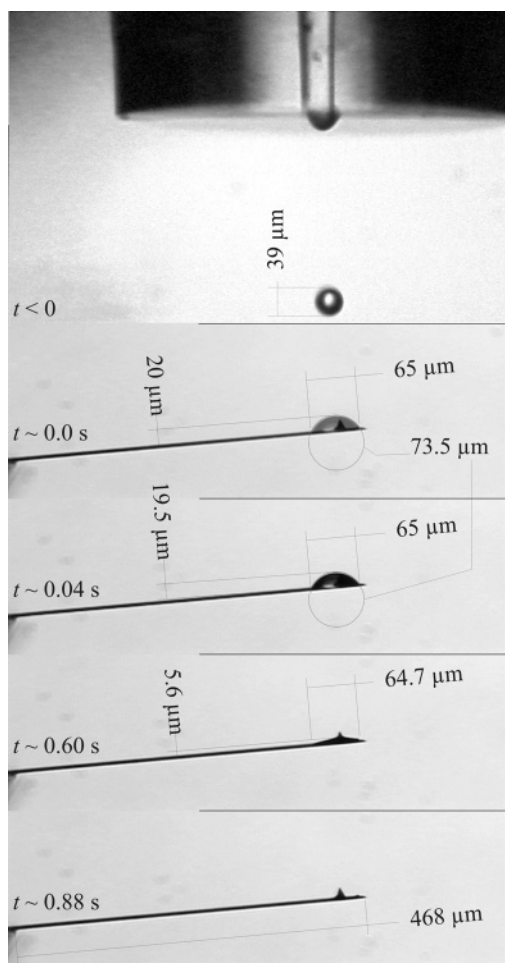*J. Phys. Chem. B, Vol. 109, No. 1, 2005* **259**

Figure 7. Typical sequence of five microscope images showing the generation of a water drop of 39 μm diameter (top), its deposition on the free end of a cantilever, and the evaporation process. Dimensions of the cantilever length, of the falling drop diameter, and of the sessile drop contact diameters and heights are indicated together with the corresponding times. The employed cantilever is a stiff one and has a tip, which protrudes by 15 μm.
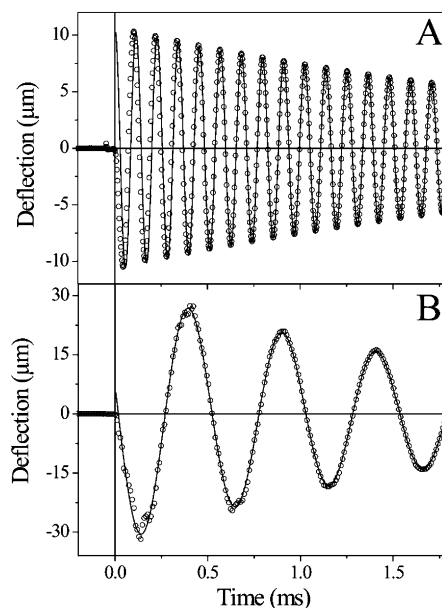

Figure 8. Cantilever deflection versus time during the impact of a drop at the free end of a cantilever. (A) Drop properties: initial mass $m_i = 2.96 \times 10^{-11}$ kg, drop diameter = 39 μm, impact velocity $v_0 = 2.0$ m/s. Cantilever properties: $l_0 = 470$ μm, $w = 50$ μm, $d = 2$ μm, $f_0 = 11.86$ kHz. Negative deflection indicates that the cantilever is bent downward, positive indicates an upward bending. Circles represent the cantilever deflection. Continuous lines represent a fit of eq 4 to the experimental curve ($A_0 = 10.7$ μm, $f_i = 8.785$ kHz, $\tau_d = 2.78$ ms, $\varphi = -1.6$, $\alpha = 2.8 \times 10^{-11}$ kg/s). (B) Drop properties: Initial mass $m_i = 2.76 \times 10^{-11}$ kg, drop diameter = 40 μm, impact velocity $v_0 = 2.0$ m/s. Cantilever properties: $l_0 = 750$ μm, $w = 100$ μm, $d = 0.89$ μm, $f_0 = 2.12$ kHz. The fit of eq 2 to the experimental curve gives $A_0 = 32.8$ μm, $f_i = 1.975$ kHz, $\tau_d = 1.95$ ms, $\varphi = -0.21$, $\alpha = 7 \times 10^{-11}$ kg/s.

at the bottom (Figure 8B) is for a soft, OTS-coated, and tipless cantilever, hit by a drop at a distance of 450 μm from the base. The drop contact angle after equilibration is about 101°.

In the following, negative times are for drops before impact and positive times are for drops after impact. The stiff cantilever (Figure 8A) is in its resting position at zero deflection until the approaching drop touches the apex of the tip at $t = -0.05$ ms. Surprisingly, the cantilever at first bends ~500 nm upward, which might be due to a capillary attraction exerted by the drop on the cantilever tip. At $t = 0$ ms, the drop momentum starts to be transmitted to the cantilever, as indicated by the sharply decreasing deflection (downward bending of the cantilever). After $t = 0.8$ ms, the total momentum of the drop is transmitted to the cantilever, and the experimental curve and the fit with eq 4 begin to overlap (clearly visible when zooming on single oscillations of the graph).

The time resolution of the measurement is given by the inverse resonance frequency of the cantilever, which is about 0.085 ms in our case and is longer than the inner-drop oscillation. Therefore, we are not able to resolve further details of the impact dynamics, but these might be revealed by cantilevers of higher resonance frequency.

There are two ways of determining the spring constant from the resonance frequency f_i and the initial mass of the drop m_i,

depending on whether we know the resonance frequency f_0 or not. If we know f_0, we can combine eqs 8 and 9 to express K only in terms of m_i, f_0, and f_i

$$K = \frac{m_i}{4\pi^2}\left(\frac{1}{f_i^2} - \frac{1}{f_0^2}\right) \qquad (40)$$

which makes it thus independent of the form of the cantilever. Otherwise, the experimental curve has to be fitted by eq 4 to obtain A_0 and f_i. Inserting them in eq 7 allows us to find m^*, and then using eq 5, we can determine K. This procedure is also independent of the form of the cantilever.

For the validation of our spring constant calibration procedure, we use a cantilever with a known spring constant $K = 0.20$ N/m and resonance frequencies $f_0 = 11.86$ kHz and $f_i = 8.785$ kHz. We insert these values in eq 40 and obtain $m_i = 3.0$ (± 0.4) $\times 10^{-11}$ kg. This is close to the value of the masses of 3.1 (± 0.2) $\times 10^{-11}$ kg of the falling drop and 3.0 (± 0.3) $\times 10^{-11}$ kg of the sessile drop determined from averages, however, of video microscope images. The three values differ by only 4%. Practically, it is easier to determine the mass of the falling or sessile drop with the video microscope.

Let us take a similar cantilever as before ($K = 0.20$ N/m) and apply the first method described here. We use the value $m_i = 3.0 \times 10^{-11}$ kg, calculated from the microscope image, and substitute it in eq 40, obtaining $K = 0.20$ N/m. Applying the second method, we have to fit the experimental curve to obtain the parameters: The fit gives $A_0 = 10.7$ μm and $f_i = 8.785$ kHz. Inserting these values in eq 7, we get $m^* = 10.5 \times 10^{-11}$ kg, and substituting this value in eq 5, we get $K = 0.30$ N/m.
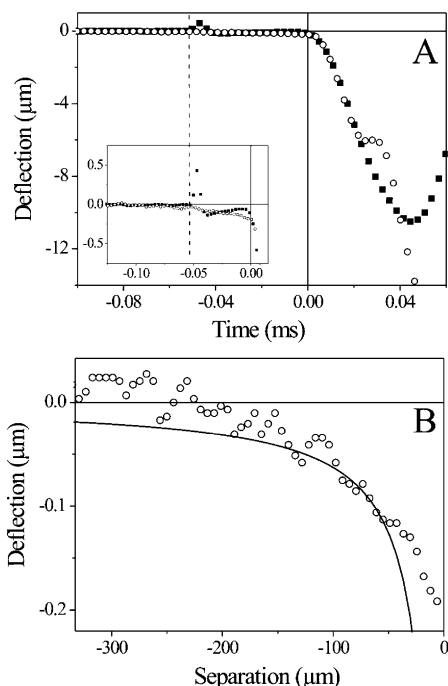
Figure 9. (A) Detail of the two deflection curves of Figure 9. Black boxes represent the stiff cantilever, hollow circles the soft cantilever. The dashed line represents the contact time between drop and tip (capillary attraction) as calculated from the tip size (15 μm) and the velocity of the drop ($v_0 = 2$ m/s). (B) Comparison between experimental (hollow circles) and theoretical (continuous line) deflection of the cantilever caused by the falling drop and air pressure. Impact is at zero separation.

The first method is more precise (reproducibility around 5%), because it makes use of the initial and final resonance frequencies, while the second method uses only the initial resonance frequency. From the fit, we are able to also extract other parameters, such as the exponential decay time constant of the initial vibration $\tau_d = 2.8$ ms and the evaporation rate $\alpha = 3.2$ (± 0.4) $\times 10^{-11}$ kg/s. Within τ_d, the evaporated mass is $\alpha \tau_d = 8.9$ (± 1) $\times 10^{-14}$ kg, which is around 0.3% of the initial mass m_i.

In Figure 8B, the soft, tipless cantilever is in its resting position at zero deflection until the approaching drop touches the cantilever. At $t = 0$ ms, the drop momentum starts to be transmitted to the cantilever, but already at $t = -0.03$ ms, the cantilever is slightly bent downward (see also Figure 9B). This is probably caused by the air pressure of the approaching drop. After $\tau_s = 0.8$ ms, the cantilever movement is described by eq 4, which implies that the total momentum of the drop has been transmitted to the cantilever, and the experimental curve shows no higher-order vibrations.

For this experiment, we used a cantilever with a known spring constant $K = 0.007$ (± 0.002) N/m. Performing the same calculations as in case A, we obtain $m_i = 3.0$ (± 0.4) $\times 10^{-11}$ kg. The mass of the falling drop is equal to 3.3 (± 0.4) $\times 10^{-11}$ kg, and the mass of the sessile drop is equal to 2.8 (± 0.4) $\times 10^{-11}$ kg, as determined from averages of side and video microscope images. Thus, in this case, 10−15% of the mass is lost during the impact of the drop. We attribute this to splashing, which in this case can be due to the different hydrophobicity of the cantilever surface (contact angle on OTS is 101°, on silicon, 62°), or by the fact that on the silicon cantilever the drop impacts on the tip before it spreads on the cantilever: The tip breaks up the drop, thus changing the impact dynamics, and prevents splashing.

For the calibration of the spring constant, we took $m_i = 2.8$ $\times 10^{-11}$ kg (sessile drop) and obtained $K = 0.006$ (± 0.001) N/m. In case f_0 is not known, the fit to the experimental curve gives $A_0 = 32.8$ μm and $f_i = 1.97$ kHz, which inserted in eqs 5 and 7 gives $K = 0.004$ (± 0.001) N/m. The exponential decay time constant is $\tau_d = 1.9$ ms, and the evaporation rate is $\alpha = 7$ (± 0.4) $\times 10^{-11}$ kg/s. Within τ_d, the evaporated mass is $\alpha \tau_d = 1.4$ (± 0.6) $\times 10^{-13}$ kg, which is around 0.5% of the initial mass m_i.

Several spring constants of cantilevers of the two types have been determined. The reproducibility of this calibration method is around 15%, which is at least as good as the accuracy of other methods (see ref 31 for a recent review). Calibrating the spring constant of AFM cantilevers by the shift in resonance frequency upon deposition of a liquid drop of known mass is an alternative to conventional methods. It is particularly suited for large cantilevers, but it is not applicable to cantilevers with dimensions $w \leq 2a$ and $l_0 \ll a$.

4.1.2. Impact Dynamics of Drops. The impact dynamics between drop and cantilever has been analyzed in more detail (Figure 9A). Both deflection curves of Figure 8 are plotted in the same graph, starting at a certain time before contact. Completion of momentum transfer is at $t = 0$ for both cantilevers. The stiff cantilever with the 15-μm tip is already touched by the drop at time $t = -0.05$ ms. The cantilever snaps upward and penetrates ∼500 nm into the drop (insert of Figure 9A): This might be due to capillary attraction between the drop and the tip. At $t = -0.4$ ms, the cantilever returns to its equilibrium position and stays so until momentum transfer is completed. The soft cantilever without a tip, on the contrary, starts to bend downward before drop impact, and at $t = 0$, it is deflected by ∼−200 nm. We attribute this to the air pressure exerted on the cantilever by the approaching drop. The Stokes friction of a spherical drop approaching the cantilever is given by[32,33]

$$F_{\text{drop}} = 6\pi\eta \frac{R^2}{h} v_0 \tag{41}$$

where $\eta = 1.86 \times 10^{-5}$ kg m^{-1} s^{-1} is the viscosity of the air, $R = 20$ μm is the radius of the drop, h is the separation between drop and cantilever, and $v_0 = 2$ m/s is the velocity of the falling drop. This is compensated by the elastic response of the cantilever

$$F_{\text{CL}} = Kz \tag{42}$$

For $t < 0$, we have $z \ll h$. Combining eqs 41 and 42, we get the deflection as a function of drop−cantilever separation

$$z = 6\pi\eta \frac{R^2}{K} v_0 \frac{1}{h} \tag{43}$$

By comparing experimental and theoretical deflections (Figure 9B), an acceptable agreement was found. When considering the simplicity of the treatment, differences at separations below 30 μm are not surprising: The calculated Stokes friction is for a rigid sphere, while the drop is a deformable object.

4.2. Drop in the Middle of the Cantilever. *4.2.1. Evaporation of Drops.* For monitoring the evaporation of a drop, we used soft cantilevers to increase sensitivity, and we focused on the time scale $t > \tau_d$. We deposited water drops on bare silicon, on gold-coated silicon, and on OTS-coated silicon cantilevers. Contact angles on silicon varied between 38° and 70°, on gold between 51° and 55°, and on OTS-coated silicon between 82°
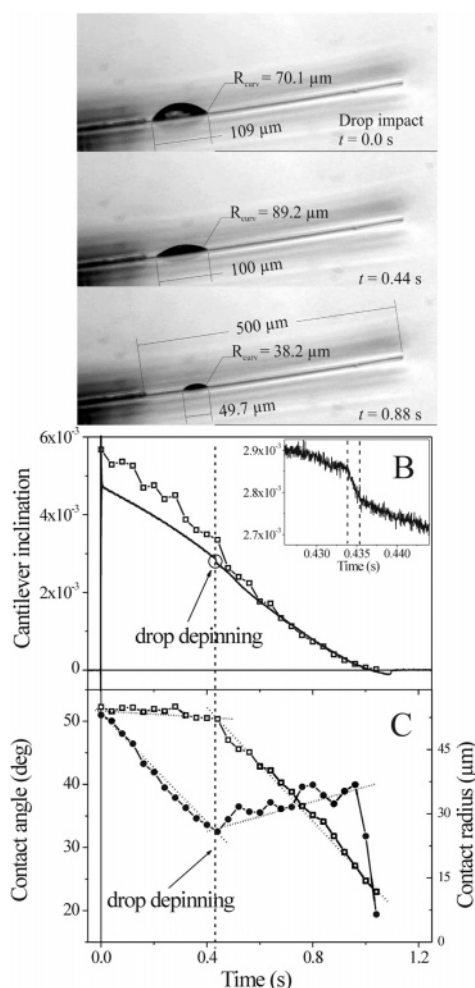
Microdrops on AFM Cantilevers

J. Phys. Chem. B, Vol. 109, No. 1, 2005 **261**

Figure 10. (A) Three video microscope images taken just after equilibration at $t \approx 0$, at $t = 0.44$ s, and at $t = 0.88$ s after impact. (B) Measured (continuous line) and calculated (hollow squares) inclination of the cantilever. Drop properties: initial mass $= 1.37 \times 10^{-10}$ kg, initial radius of falling drop $R = 31.8$ μm, initial contact angle $\Theta = 51°$, and contact radius $a = 55$ μm. Cantilever properties: $l_0 = 500$ μm, $w = 100$ μm, $d = 0.95$ μm, $f_0 = 4.75$ kHz, $K = 0.03$ N/m. A positive inclination indicates that the cantilever bends toward the drop (upward). The circle highlights a depinning event; the inset shows it in more detail between the two dashed lines. (C) Contact angle (full circles) and contact radius (hollow squares). The dashed line shows the simultaneous kink in the curves.

and 101°. We call the bending of the cantilever "static" because the drop movements caused by the evaporation take place at a much slower time scale than the inverse of the resonance frequency of the cantilever. Therefore, we assume the cantilever to be in equilibrium at any stage with respect to a given drop shape.

A typical inclination signal measured with a drop deposited close to the base of a bare silicon cantilever is shown in Figure 10, together with three representative video images taken at different stages of the evaporation (Figure 10A). The continuous line represents the experimental inclination of the cantilever. In this case, we plot inclination rather than deflection because for $x > x_0 + a$, the inclination is constant, while the deflection changes along the length of the cantilever and depends on the precise position of the drop.

The open boxes in Figure 10B are values calculated by eq 37 with a and Θ as obtained by video microscopy. As parameters, the surface tension of water $\gamma = 0.072$ N/m², Young's modulus of the cantilever, $E = 180$ GPa, and
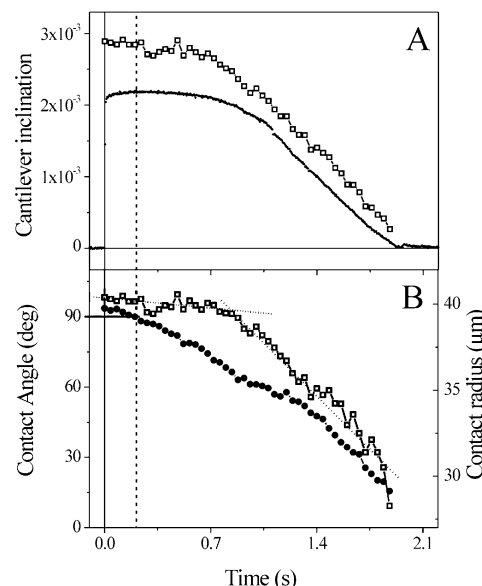

Figure 11. (A) Measured (continuous line) and calculated (hollow squares) inclination of the cantilever. Drop properties: initial mass $= 1.53 \times 10^{-10}$ kg, initial radius of falling drop $R = 33.2$ μm, initial contact angle $\Theta = 93°$, and contact radius $a = 41$ μm. Cantilever properties: $l_0 = 750$ μm, $w = 100$ μm, $d = 0.95$ μm, $f_0 = 2.38$ kHz, $K = 0.009$ N/m. (B) Contact angle (full circles) and contact radius (hollow squares). The dashed line indicates the time when the contact angle $\Theta = 90°$.

$I = wd^3/12 = 5.89 \times 10^{-24}$ m⁴ were inserted. Calculated inclination values show the same tendency as the experimental signal, but are around 20% higher than experimental values at the beginning. The difference gets smaller during the evaporation process. If the simplicity of the theory and the uncertainty of several parameters (in particular, the thickness of the cantilever und thus I) are considered, this is a good agreement. One effect which could lead to a reduction of the measured signal is a possible bending of the cantilever in the lateral direction (i.e., across w). This would make the cantilever stiffer and increase its spring constant.[34]

In addition to the monotonic decay of the inclination, another feature highlights the sensitivity of the method. At $t = 433.8$ ms, the slope of the inclination signal changes. This reflects a depinning event of the three-phase contact line. Up to this point, the evaporation was characterized by a constant contact radius and a linearly decreasing contact angle (Figure 10C). After the three-phase contact line is no longer pinned, the contact radius decreases with time, while the contact angle remains constant. This transition between constant contact radius and constant contact angle takes from $t = 433.8$ ms to $t = 435.6$ ms.

The evaporation of a water drop deposited close to the base of an OTS-coated silicon cantilever is shown in Figure 11A. The continuous line represents the experimental inclination of the cantilever and the open boxes represent the values calculated by eq 37 with a and Θ as obtained by video microscopy (Figure 11B). Calculated inclination values show the same tendency as the experimental signal, but are around 30% higher than experimental values. The drop forms a contact angle $\Theta > 90°$ at $t = 0$ (Figure 11B). At $t = 200$ ms, $\Theta = 90°$, and in accordance with eq 37, the inclination of the cantilever reaches a maximum. During all the evaporation, the contact angle continuously decreases, while the contact radius is at first constant, until the drop depins at $t = 800$ ms.

Usually, the last 0.5−0.7 s of the evaporation process show a linearly decreasing inclination signal almost to the end. For drops so small that the whole evaporation process lasts only
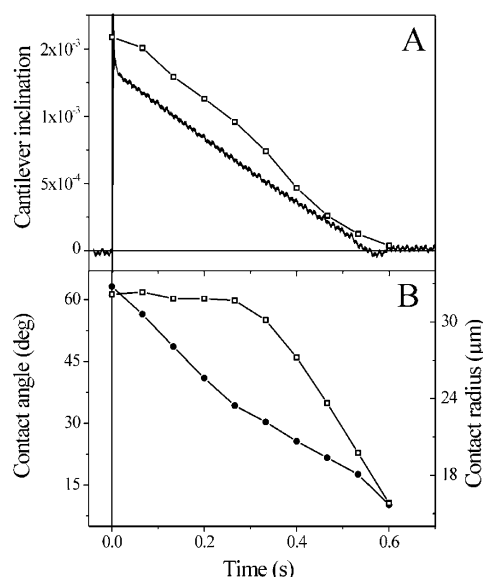
Figure 12. (A) Measured (continuous line) and calculated (hollow squares, eq 37) inclination of the cantilever. Drop properties: Initial mass $= 3.62 \times 10^{-11}$ kg, initial radius of falling drop $R = 23.1$ μm, initial contact angle $\Theta = 63°$, and contact radius $a = 32$ μm. Cantilever properties: $l_0 = 500$ μm, $w = 100$ μm, $d = 0.89$ μm, $f_0 = 4.61$ kHz, $K = 0.024$ N/m. (B) Contact angle (full circles) and contact radius (hollow squares).
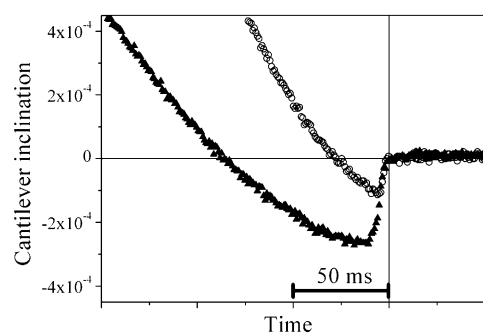

Figure 13. End of inclination curves of two cantilevers with different wettabilities. Black triangles: initial contact angle of water drop on cantilever $\Theta_i = 88°$, initial drop mass $m_i = 1.72 \times 10^{-10}$ kg, drop evaporation time $\tau_e = 1.8$ s. Open circles: $\Theta_i = 51°$, $m_i = 1.34 \times 10^{-10}$ kg, $\tau_e = 0.9$ s. Curves have been horizontally shifted in order to have a coincident end of the evaporation time.

0.5 s, the whole inclination signal is a linear decrease (Figure 12). Here, calculated and measured inclination values are off by typically 15%.

4.2.2. End of Evaporation Process. In the majority of the experiments, we observed that at the end of the evaporation the cantilever bends away from the drop, leading to a negative inclination, though the precise shape of the signal varied from cantilever to cantilever (Figure 13). We present here the last part of the evaporation process for two cantilevers with different wettabilities: The initial contact angles are 88° for the more hydrophobic one (OTS-coated) and 51° for the more hydrophilic one (bare silicon). The end of evaporation is set for both curves arbitrarily to $t = 0$, although τ_e of the hydrophilic cantilever is ~0.9 s and τ_e of the hydrophobic cantilever is ~1.8 s (due to a larger initial drop mass).

Such a bending of the cantilever away from the drop can be understood assuming that a thin layer of water remains on the surface for 0.1−0.3 s, perhaps pinned on the rim because of microscopic inhomogeneities or contaminations on the cantilever surface. In this case, the contact angle is negligibly small (Figure
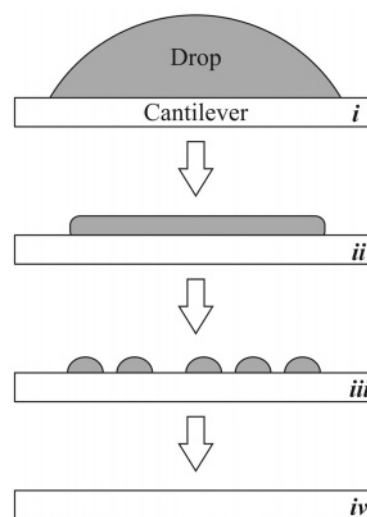

Figure 14. Tentative interpretation for the negative inclination of the cantilever arising at the last stages of drop evaporation. (i) Drop is pinned while Θ decreases, (ii) $\Theta \approx 0$, and only a thin water layer covers the cantilever, (iii) layer might also break up and microdroplets are formed, (iv) evaporation is complete.

14), and the last terms in eq 37 can dominate. Even if this layer is not continuous, but at some stage breaks up into small droplets or liquid patches, the second term in eq 37 becomes more important, because the contact radius becomes comparable to the cantilever thickness.

Such a liquid layer remaining at the surface could be a few nanometers thick so that solid−liquid and solid−vapor interfaces are still present. The evaporation of this layer could be slowed due to surface forces. For example, the van der Waals force between the solid−liquid and liquid−vapor interfaces is repulsive, which could reduce the evaporation rate.

5. Conclusions

A new AFM cantilever spring constant calibration method is presented. A drop of water with a known mass is dispensed onto the free end of a cantilever, thereby exciting it by its momentum transfer. By recording and fitting the resulting damped oscillation, several parameters can be obtained. Among these are the initial evaporation rate of the drop, the amplitude of the excited oscillation, and the new damped resonance frequency. The spring constant is obtained independently of the geometry and the material properties of the cantilever. Also, the air pressure exerted by the drop on the cantilever before impact can be detected.

A water drop deposited on one face of a cantilever causes it to bend. The main reason for bending is the Laplace pressure inside the drop and the surface tension of the liquid acting at the rim. In addition, the change in surface stress at the solid−liquid interface and line tension can lead to a bending. Analytical expressions are derived to describe all contributions. It is shown that an AFM cantilever can be used to analyze the evaporation of a water drop with high sensitivity and time resolution by recording the cantilever inclination versus time. The results obtained with water indicate that during the last stage the evaporation process is slowed and a thin layer of water remains on the surface for $t \gg 0.1$ s.

Microdrops on AFM Cantilevers

J. Phys. Chem. B, Vol. 109, No. 1, 2005 **263**

References and Notes

(1) Birdi, K. S.; Vu, D. T.; Winter, A. *J. Phys. Chem.* **1989**, *93*, 3702−3703.

(2) Bourges-Monnier, C.; Shanahan, M. E. R. *Langmuir* **1995**, *11*, 2820−2829.

(3) Cachile, M.; Benichou, O.; Cazabat, A. M. *Langmuir* **2002**, *18*, 7985−7990.

(4) Hu, H.; Larson, R. G. *J. Phys. Chem. B* **2002**, *106*, 1334−1344.

(5) Picknett, R. G.; Bexon, R. *J. Colloid Interface Sci.* **1977**, *61*, 336350.

(6) Rowan, S. M.; Newton, M. I.; McHale, G. *J. Phys. Chem.* **1995**, *99*, 13268−13271.

(7) Rowan, S. M.; McHale, G.; Newton, M. I.; Toorneman, M. *J. Phys. Chem. B* **1997**, *101*, 1265−1267.

(8) McHale, G.; Rowan, S. M.; Newton, M. I.; Banerjee, M. K. *J. Phys. Chem. B* **1998**, *102*, 1964−1967.

(9) Deegan, R. D. *Phys. Rev. E* **2000**, *61*, 475−485.

(10) Deegan, R. D.; Bakajin, O.; Dupont, T. F.; Huber, G.; Nagel, S. R.; Witten, T. A. *Phys. Rev. E* **2000**, *62*, 756−765.

(11) Deegan, R. D.; Bakajin, O.; Dupont, T. F.; Huber, G.; Nagel, S. R.; Witten, T. A. *Nature* **1997**, *389*, 827−829.

(12) Pham, N. T.; McHale, G.; Newton, M. I.; Carroll, B. J.; Rowan, S. M. *Langmuir* **2004**, *20*, 841−847.

(13) Uno, K.; Hayashi, K.; Hayashi, T.; Ito, K.; Kitano, H. *Colloid Polym. Sci.* **1998**, *276*, 810−815.

(14) McKenna, L.; Newton, M. I.; McHale, G.; Lucklum, R.; Schroeder, J. *J. Appl. Phys.* **2001**, *89*, 676−680.

(15) McHale, G.; Erbil, H. Y.; Newton, M. I.; Natterer, S. *Langmuir* **2001**, *17*, 6995−6998.

(16) Kern, R.; Müller, P. *Surf. Sci.* **1992**, *264*, 467−494.

(17) White, L. R. *J. Colloid Interface Sci.* **2003**, *258*, 82−96.

(18) Spaepen, F. *J. Mech. Phys. Solids* **1996**, *44*, 675−681.

(19) von Bahr, M.; Tiberg, F.; Zhmud, B. *Langmuir* **2003**, *19*, 10109−10115.

(20) Rioboo, R.; Marengo, M.; Tropea, C. *Exp. Fluids* **2002**, *33*, 112−124.

(21) Rein, M. *Fluid Dyn. Res.* **1993**, *12*, 61−93.

(22) Butt, H.-J.; Siedle, P.; Seifert, K.; Fendler, K.; Seeger, T.; Bamberg, E.; Weisenhorn, A. L.; Goldie, K.; Engel, A. *J. Micros. (Oxford)* **1993**, *169*, 75−84.

(23) Butt, H.-J.; Jaschke, M. *Nanotechnology* **1995**, *6*, 1−7.

(24) Sarid, D. *Scanning Force Microscopy*; Oxford University Press: New York, 1991.

(25) Cleveland, J. P.; Manne, S.; Bocek, D.; Hansma, P. K. *Rev. Sci. Instrum.* **1993**, *64*, 403−405.

(26) Stoney, G. G. *Proc. R. Soc. London, Ser. A* **1909**, *82*, 172−175.

(27) Cappella, B.; Dietler, G. *Surf. Sci. Rep.* **1999**, *34*, 1−104.

(28) Gould, S. A. C.; Drake, B.; Prater, C. B.; Weisenhorn, A. L.; Manne, S.; Kelderman, G. L.; Butt, H.-J.; Hansma, H.; Hansma, P. K.; Magonov, S.; Cantow, H. J. *Ultramicroscopy* **1990**, *33*, 93−98.

(29) Preuss, M.; Butt, H.-J. *Langmuir* **1998**, *14*, 3164−3174.

(30) Hutter, J. L.; Bechhoefer, J. *Rev. Sci. Instrum.* **1993**, *64*, 1868−1873.

(31) Burnham, N. N.; Chen, X.; Hodges, C. S.; Matei, G. A.; Thoreson, E. J.; Roberts, C. J.; Davies, M. C.; Tendler, S. J. B. *Nanotechnology* **2003**, *14*, 1−6.

(32) Brenner, H. *Chem. Eng. Sci.* **1961**, *16*, 242−251.

(33) Chan, D. Y. C.; Horn, R. G. *J. Chem. Phys.* **1985**, *83*, 5311−5324.

(34) Sader, J. E. *J. Appl. Phys.* **2001**, *89*, 2911−2921.